Effect of the Hydrodynamic Bearing on Rotor/Stator Contact in a Ring-Type Ultrasonic Motor

Takashi Maeno and David B. Bogy. *Member, IEEE*

Abstract—**A hybrid numerical analysis that includes the hydrodynamic bearing effect and elastic contact in a ring-type ultrasonic motor is presented. The two-dimensional time-dependent compressible Reynolds equation is solved numerically by a second order time accurate, noniterative, factored implicit finite difference algorithm. The rotor deformation is described by a one dimensional Green's function obtained by calculating the actual rotor deformation due to a normal point load using a finite element elastic analysis code. The contact problem is solved by an iteration method so that the contact condition and the hydrodynamic bearing condition are satisfied simultaneously. The results show that the hydrodynamic bearing effect, especially the squeeze effect, is significant for ultrasonic frequency contact of the rotor and stator. Surface roughness, contact area, and normal vibrating speed of the stator are important parameters in the hydrodynamic bearing. The disagreement between the friction coefficient needed in the numerical analysis and the experimentally measured one in the previous study, which did not include the air bearing, is settled as well.**

I. Introduction

ONE of the most important points for designing an ultrasonic motor is the control of a dynamic contact behavior between a rotor and a stator. Maeno *et al.* [1], [2] calculated the mechanical characteristics of the ring type ultrasonic motor by using the JNIKE3D FE code. The elastic contact of the rotor/stator, considering the shear deformation of bodies by using a static friction coefficient μ_s and a dynamic friction coefficient μ_d, was simulated. A complex distribution of the stick and slip areas within the contact region was shown. Motor performance, including the T–N curve, power loss, and efficiency, was calculated as well. By considering the initial displacement of the rotor/stator, they obtained results in good agreement with the experimental results. But the dynamic friction coefficient μ_d needed in the numerical analysis was different from the experimentally measured one.

The maximum operating torque $T_{\max}$ of the ultrasonic motor can be calculated by

$$T_{\max} = \mu_d L r \tag{1}$$

where L is the total load and r is the contact radius. At this torque, the entire contact area slips and the rotational speed of the rotor cannot be determined. If we accept the dynamic friction coefficient ($\mu_d = 0.7$) measured in our previous study, the maximum torque must be 0.30 N·m when $L = 14.7$ N and $r = 29$ mm. But the actual maximum torque was 0.17 N·m. In order to obtain a T–N curve in agreement with the measured curve, we needed to use a lower friction coefficient ($\mu_d = 0.4$). The purpose of this continuation study is to investigate this difference of friction coefficients by introducing air bearing effects into the contact interface.

Analyses of compressible gas films with a high frequency variation of film thickness have been undertaken by many researchers of hydrodynamic bearings [3],[4]. These results suggest the possibility that the hydrodynamic bearing may play an important roll in the high frequency contact between the rotor and stator of the ultrasonic motor. In this study, we introduce the hydrodynamic bearing into the contact between the rotor and stator in a ring-type ultrasonic motor.

In section two, a hybrid numerical analysis scheme for solving the elastic contact and the hydrodynamic bearing simultaneously is presented. The two dimensional time-dependent compressible Reynolds equation is solved numerically by a second order time accurate, noniterative, factored implicit finite difference algorithm derived by White and Nigam [5]. The rotor deformation is described by a one dimensional Green's function obtained by calculating the actual rotor deformation due to a normal point load using the finite element elastic analysis code JNIKE3D. The contact problem is solved by an iteration method so that the contact condition and the hydrodynamic bearing condition are satisfied simultaneously.

In section three, the calculated results are shown. The hydrodynamic bearing effect, especially the squeeze effect, is found to be significant for ultrasonic frequency contact of the rotor and stator. Surface roughness, contact area, and normal vibrating speed of the stator are important parameters for the hydrodynamic bearing. The disagreement between the friction coefficient needed in the numerical analysis and the experimentally measured one in the previous study is explained.

II. Formulation

A. Reynolds Lubrication Equation

The first order corrected for boundary slip compressible Reynolds lubrication equation for a finite width bearing has

Manuscript received January 14, 1992; revised May 11, 1992; accepted May 26, 1992. This work was supported by the Computer Mechanics Laboratory and by Canon Inc.

T. Maeno was with the Computer Mechanics Laboratory, Department of Mechanical Engineering, University of California, Berkeley, CA 94720, and is now with Canon, Inc., 3-30-2, Shimomaruko, Ohta-ku, Tokyo 146, Japan.

D. B. Bogy is with the Computer Mechanics Laboratory, Department of Mechanical Engineering, University of California, Berkeley CA 94720.

IEEE Log Number 9203443.

the form

$$\frac{\partial}{\partial x}\left[ph^3\frac{\partial p}{\partial x}\left(1+\frac{6m}{ph}\right)\right]+\frac{\partial}{\partial y}\left[ph^3\frac{\partial p}{\partial y}\left(1+\frac{6m}{pm}\right)\right] = \Delta\frac{\partial}{\partial x}[ph]+\Delta\frac{\partial}{\partial y}[ph]+\sigma\frac{\partial}{\partial t}[ph] \quad (2)$$

where $p(x,y,t)$ is the pressure, $h(x,y,t)$ is the film thickness, Δ is the bearing number, σ is the so-called "squeeze" number, and m is the Knudsen number that relates the mean free path of the gas molecules to the minimum film thickness.

Defining $Z = ph$, linearizing (2), and introducing a rectangular mesh of $p \times q$ grid points within the bearing region, we can write the finite difference form of (2) [5] as

$$[1-L]\Delta Z^*_{i,j} = \xi_{i,j} \quad (i=0,p-1,j=0,q-1) \quad (3)$$

and

$$[1-\bar{L}]\Delta Z^{(n+1)}_{i,j} = \Delta Z^*_{i,j} \quad (i=0,p-1,j=0,q-1) \quad (4)$$

where

$$\Delta Z^{(n+1)}_{i,j} = Z^{(n+1)}_{i,j} - Z^{(n)}_{i,j}$$

$$L = a[h(z+6m)\delta_{xx} + (2hZ_x - h_xZ - \Delta)\delta_x + hZ_{xx} - h_xZ_x - h_{xx}(2Z+6m)]$$

$$\bar{L} = a[h(z+6m)\delta_{yy} + (2hZ_y - h_yZ - \Delta)\delta_y + hZ_{yy} - h_yZ_y - h_{yy}(2Z+6m)]$$

$$\xi = a[[(Z+6m)(Z_{xx}+Z_{yy}) + (Z_x^2+Z_y^2)](h^{(n+1)}+h^{(n)}) - Z[Z_x(h_x^{(n+1)}+h_x^{(n)}) + Z_y(h_y^{(n+1)}+h_y^{(n)})] - Z(Z+6m)[h_{xx}^{(n+1)}+h_{xx}^{(n)}+h_{yy}^{(n+1)}+h_{yy}^{(n)}] - 2[\Delta Z_x + \Delta Z_y]]$$

$$a = \frac{\Delta t}{2\sigma}$$

where δ_x and δ_y are finite difference operators, superscript (n) and $(n+1)$ are time step (n) and $(n+1)$, respectively, and subscript x, y, and t are partial differentiation.

Since L only involves operators in the x-direction, and similarly $\bar{L}$ in the y-direction, (3) represents a set of p simultaneous equations for the p variables $\Delta Z^*_{i,j}(i=0,p-1)$ for each index j, and (4) represents a set of q simultaneous equations for the q variables $\Delta Z^{(n+1)}_{i,j}(j=0,q-1)$ for each index i. Consequently, the problem of obtaining the solution of the Reynolds equation reduces to the following:

1) determine the values of $Z^{(n)}_{i,j}, h^{(n)}_{i,j}, h^{(n+1)}_{i,j}$, and their derivatives, and calculate the values of $\xi_{i,j}$
2) for each j, invert the $p \times p$ square matrix in (3) and obtain values of $\Delta Z^*_{i,j}$ using those of $\xi_{i,j}$
3) for each i, invert the $q \times q$ square matrix in (4) and obtain values of $\Delta Z^{(n+1)}_{i,j}$ using those of $\Delta Z^*_{i,j}$
4) obtain the solution

$$p^{(n+1)}_{i,j} = \frac{Z^{(n+1)}_{i,j}}{h^{(n+1)}_{i,j}} = \frac{Z_{i,j}+\Delta Z^{(n+1)}_{i,j}}{h^{(n+1)}_{i,j}}.$$

Then we can obtain the pressure distribution p within the bearing region at the time step $(n+1)$ from the given $Z^{(n)}_{i,j}, h^{(n)}_{i,j}$, and $h^{(n+1)}_{i,j}$.

B. Stator Vibration and Rotor Displacement

When the traveling wave is moving to the negative x-direction, the normal displacement of the stator at the top of the teeth, W_{Sn}, is

$$W_{Sn}(i) = A_S\cos 2\pi(ft + \frac{\Delta x(i-1)}{\lambda})$$
$$\Delta x = \frac{\lambda}{N} \quad (5)$$

where, A_S is the normal amplitude, f is the frequency, and λ is the wave length of the stator traveling wave. Also, N is the division number of the rotor in the circumferential direction through one wave length. On the other hand, the tangential displacement W_{St} is

$$W_{St}(i) = B_S\sin 2\pi(ft + \frac{\Delta x(i-1)}{\lambda}) \quad (6)$$

where, B_S is the tangential amplitude. Also, the tangential velocity of the stator V_{St} is

$$V_{St}(i) = \frac{\partial W_{St}}{\partial t} = 2\pi f B_S\cos 2\pi(ft + \frac{\Delta x(i-1)}{\lambda}). \quad (7)$$

The rotor contacts with the stator at the top of this traveling wave. Maeno et. al. [1] solved for the deformation of the three dimensional rotor contacting the stator teeth by using the finite element code JNIKE3D. But we do not have to model the full rotor to solve the hybrid problem between the hydrodynamic bearing and contact because only the normal displacement and the tangential velocity of the rotor are needed. In this study, we introduce a one dimensional Green's function of the rotor obtained by calculating the deformation of the actual three dimensional rotor corresponding to a normal point load using a FE code. After obtaining the one dimensional Green's function, we have only to use this function to solve the contact problem. If the discrete form of the Green's function is denoted by $G_{i,j}$, which represents the normal displacement of point j when a unit force is applied at point i, the normal displacement of the rotor at point j is

$$W_R(j) = \sum_{i=1}^{N} G_{i,j}f_i \quad (8)$$

where, f_i is a point force applied at point i. The tangential velocity of the rotor, V_R, is calculated from the rotating speed. A local change of the rotor velocity due to the shear deformation of the rotor is neglected because the local change is small compared to the rotating speed. The relative velocity V_{rel} between the rotor and stator is obtained by

$$V_{\text{rel}} = V_R - V_{St} \quad (9)$$

C. Hybrid Analysis of the Contact Problem Including the Hydrodynamic Bearing Effect

If the contact pressure, the hydrodynamic bearing pressure, and the deformation of the stator teeth are given, the rotor

deformation can be calculated using equations (5) and (8) by an iteration method so as to satisfy the contact condition,

$$f_i > 0 \text{ and } W_R = W_{Sn} \text{ at contact grids}$$
$$f_i = f_l \text{ and } W_R > W_{Sn} \text{ at noncontact grids} \quad (10)$$

where f_l is the resultant force of the hydrodynamic bearing pressure.

On the other hand, if the spacing between each stator tooth and the rotor spring at time (n) and $(n+1)$, the relative velocity at time (n) and $(n+1)$, and the pressure at time (n) are given, the hydrodynamic pressure at time $(n+1)$ can be obtained from (3) and (4). So, we can obtain by iteration the hybrid solution of the contact problem and the hydrodynamic bearing problem by solving each problem in order.

When the spacing between two bodies is zero, we cannot solve the Reynold's equation because the hydrodynamic pressure becomes unbounded. But the actual surface of a body has roughness. The surfaces of two bodies contact in a particular area, the so called 'real area of contact', and the rest of the area has some spacing distribution. So we assume that the spacing between two contacting bodies has a certain minimum value, H_m, that is determined by the surface roughness, in order to solve the Reynold's equation. The minimum spacing H_m is taken as the mean value of the peak to valley roughness of the two surfaces. This assumption is desirable and reasonable because it leads to a simple calculation without loosing the macroscopic effect of hydrodynamics. In this manner, we can solve the Reynold's equation with contact considering the surface roughness and retaining the finite value of hydrodynamic pressure.

Since the distribution of the N discrete nodes for the rotor/stator contact problem is one dimensional in the circumferential direction and the distribution of the $p \times q$ nodes for the hydrodynamic bearing problem within the interface area on each tooth is two dimensional, we must map the values of the variables such as p, h, W_R, W_{Sn}, and V_{rel} from one grid to the other in each problem. For this, we use linear interpolation. The pressure distribution p obtained from the hydrodynamic bearing problem is summed in the radial direction for the contact problem. On the other hand, the spacing distribution h calculated in the contact problem

$$h = W_R - W_{Sn}$$

is assumed to be uniform to the radial direction.

A flow chart of the algorithm is shown in Fig. 1. The time step Δt is selected as

$$\Delta t = \frac{T}{m}$$

where m is the integer and T is the vibration cycle of stator $(= 1/f)$(s), in order to check if the deformation and the pressure are steady by comparing with the previous cycle.

First, the displacement at the top of the stator teeth at time t due to the traveling wave is calculated by (5). Next, the rotor deformation is calculated so as to satisfy the assumed contact condition. For the initial calculation, the contact condition is assumed so that the positively displaced stator teeth contact the rotor. Then, the contact condition is checked to determine if (10) is satisfied. If it is not satisfied, the contact condition is changed and the calculation of the rotor deformation is repeated. After the contact condition is satisfied, the hydrodynamic bearing pressure between each tooth and the rotor is calculated by using the spacing at time t and $t - \Delta t$, the relative velocity at time t and $t - \Delta t$, and the pressure at time $t - \Delta t$. Since the pressure at $t - \Delta t$ is not known for the initial calculation, the value zero is used for the initial pressure. Then the convergence condition is checked for the pressure and the spacing at time t. If convergence is not obtained, we go back to the calculation of the rotor deformation and repeat the above. If convergence is achieved, then we determine if the deformation and the pressure are steady, in another words, whether or not the deformation of the rotor and the pressure distribution are sufficiently near the previous cycle. The steady deformation and the pressure distribution are the required results of the solution.

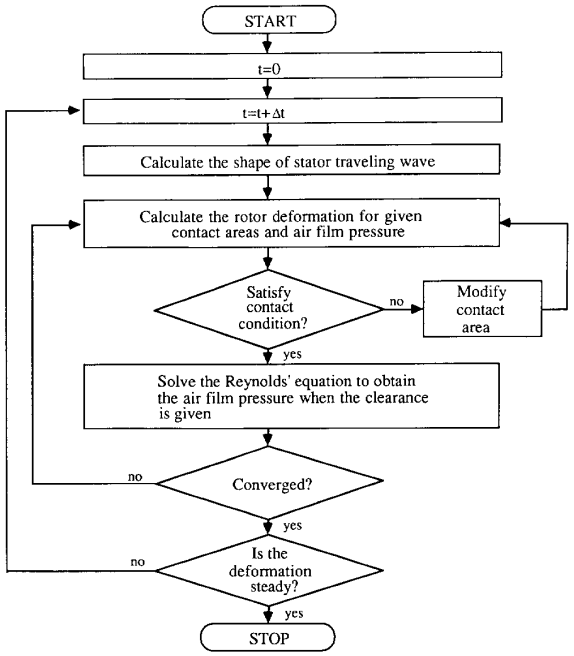

Fig. 1. Flowchart of analysis.

In order to estimate the effect of the hydrodynamic bearing, we define a hydrodynamic bearing pressure ratio α by

$$\alpha = \sum_{i=1}^{N} f_1(i) \Big/ L \quad (11)$$

where $f_1(i)$ is the hydrodynamic bearing load at node i and L is the total normal load. The ratio α indicates how much of the total load is provided by the hydrodynamic lubrication pressure. Since the friction coefficient of hydrodynamic lubrication μ_l is much smaller than μ_d

$$\mu_l \ll \mu_d$$

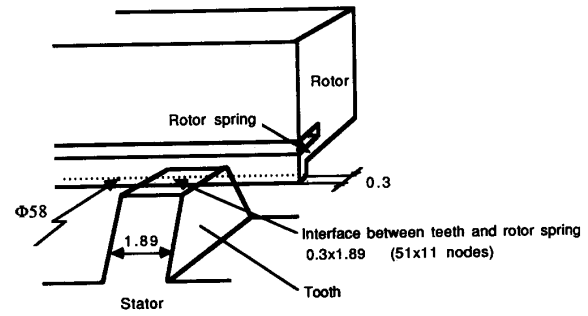

Contact diameter	58 mm
Traveling wave length	26 mm
Number of teeth per one traveling wave	9
Teeth width	1.89 mm
Rotor spring width	0.3 mm
Surface roughness	200 nm
Stator amplitude	2.0E-3 mmp-p
Rotor speed	180 mm/sec
Total load per one wave	2.45 N
Dynamic viscosity of air	0.181E-4 kg/m/sec
Atmospheric pressure	1.010E5 Pa
Mean free path of air	0.064E-6 m
Division of rotor on circumferential direction for contact analysis	181
Division of interface between stator and rotor spring	51x11

Fig. 2. Schematic view of the rotor/stator and the fundamental values used in the calculation.

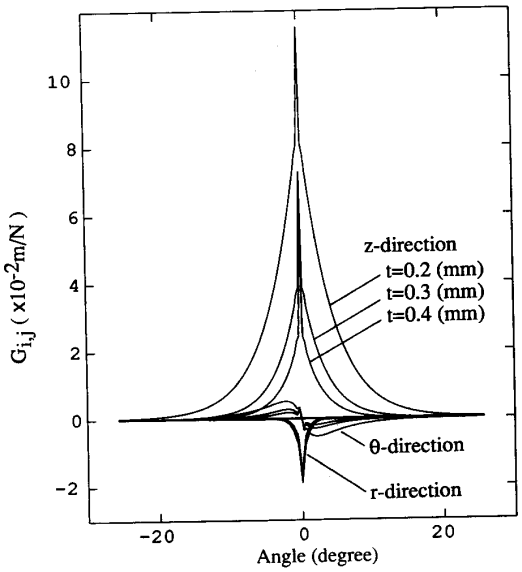

Fig. 3. Green's function of the rotor calculated by JNIKE3D FE code (2162 elements, 2721 nodes).

we can compute the maximum operating torque $T_{\max}$ by

$$T_{\max} = \mu_d(1-\alpha)Lr \tag{12}$$

instead of (1). In this equation, a high α means a low maximum torque.

III. Calculated Results

A. Fundamental Case

The calculation is applied to various design parameters. At first, the deformation and the pressure are calculated for the actual rotor/stator geometry as shown in Fig. 2, which we call the "fundamental case." One wave length of the rotor is divided into 181 nodes. Each interface between a tooth and rotor is divided into 51 × 11 nodes as well.

Fig. 3 shows the one dimensional Green's function obtained by calculating the actual rotor deformation due to a normal point load using the JNIKE3D FE code.

First, the accuracy of the solution is ascertained by doubling the mesh size. When $N = 361$ and $p \times q = 101 \times 21$, the difference of the resultant hydrodynamic pressure with the fundamental case was only 12 (mN) (see Table I). So we conclude that the division number used in the fundamental case is large enough.

Fig. 4 shows the displacement of the rotor/stator and the pressure distribution of the fundamental case. The traveling wave moves to the left and the rotor moves to the right. The upper figure shows that the rotor contacts three stator teeth at this time. The lower figure shows that the hydrodynamic bearing effect on the rotor/stator contact is significant. Since the contact period is short, the hydrodynamic bearing pressure does not decrease while the rotor and stator contact. The hydrodynamic bearing pressure ratio α of the fundamental case is 0.24. (Hydrodynamic bearing pressure ratios for various design parameters are shown in Table I.) In order to explain the disagreement of the friction coefficient used in the calculation ($\mu_d = 0.4$) and the measured one ($\mu_d = 0.7$) in the previous study [1], we need a hydrodynamic bearing pressure ratio of about 0.43. So the hydrodynamic bearing effect obtained is somewhat small for explaining the difference of μ quantitatively.

The result calculated by neglecting a shear velocity shows that the ratio α is almost the same as the one in the fundamental

TABLE I
Hydrodynamic Bearing Load and Ratio α

Changed Variables	Load (N)	Ratio
Fundamental case	0.583	0.238
p =101, q =21, N = 361	0.595	0.243
Hm =100 nm	1.179	0.481
Rotor width=0.6 mm	1.141	0.466
Teeth width=1.16 mm	0.386	0.157
Teeth width=2.31 mm	0.779	0.318
Stator frequency=3 kHz	0.192	0.078
Stator frequency=20 kHz	0.550	0.224
Stator frequency=40 kHz	0.600	0.245
Stator frequency=60 kHz	0.615	0.251
Stator frequency=100 kHz	0.630	0.257
Teeth radius=3 m	0.576	0.235
Teeth radius=6.5 m	0.585	0.239
Teeth radius=10 m	0.586	0.239

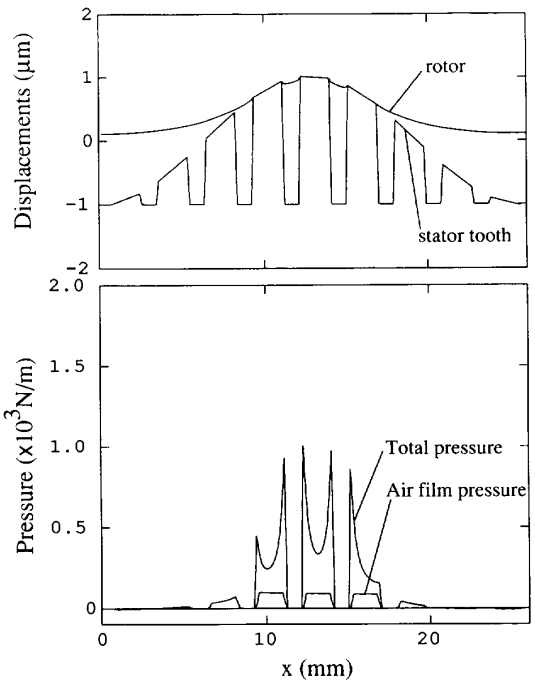

Fig. 4. Normal displacement and pressure distribution (fundamental case).

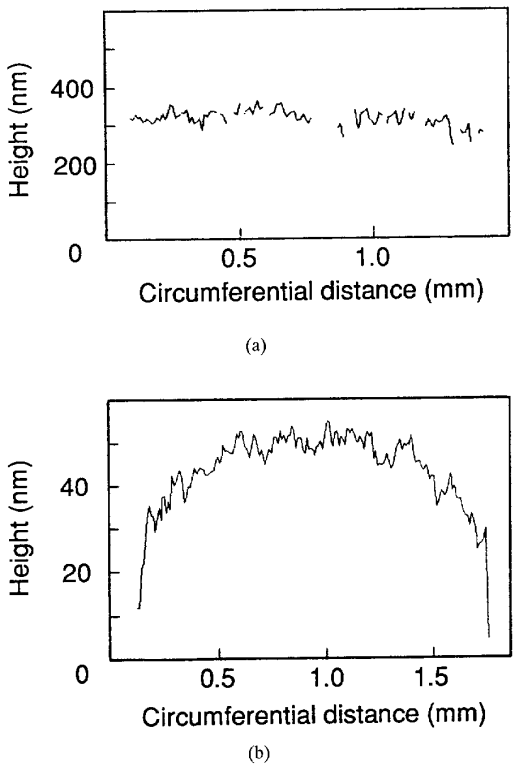

Fig. 5. Surface geometry of the rotor/stator interface. (a) Rotor spring. (b) Stator tooth.

case. So the squeeze effect, the last term in (2), is very much larger than the wedge effect, the first and the second terms in the right hand side of the equation.

B. Effect of Surface Roughness

Fig. 5 shows the surface geometry of the actual rotor/stator after driven for several hours measured by Zygo Maxim-3D. Fig. 5(a) shows the geometry of the contact interface line on the rotor. As the surface of the rotor spring has deep holes, we could not measure the whole geometry of the surface by using Zygo Maxim-3D. Fig. 5(b) shows the geometry on one tooth of the stator. In this figure, the maximum surface roughness of the rotor/stator are about 100 nm and 50 nm, respectively. This value changes due to wear, the initial surface is rougher.

Fig. 6 shows the displacement of the rotor/stator and the pressure distribution when the minimum air bearing spacing is 100 nm. The minimum spacing represents the mean clearance between the rotor and stator when they contact, in other words, a value proportional to the surface roughness. When the minimum spacing is 100 nm—meaning that the surface roughness of the rotor and stator are about 100 nm $p - p$ each—the hydrodynamic bearing pressure ratio α is up to 0.48. This result shows that the hydrodynamic bearing pressure increases when the minimum spacing decreases. In order to reduce the effect of the hydrodynamic bearing pressure, we must have a rough interface surface. The surface should be designed so that the roughness does not change due to the wear for stable motor performance, such as the T–N (torque-rotational speed) curve and efficiency.

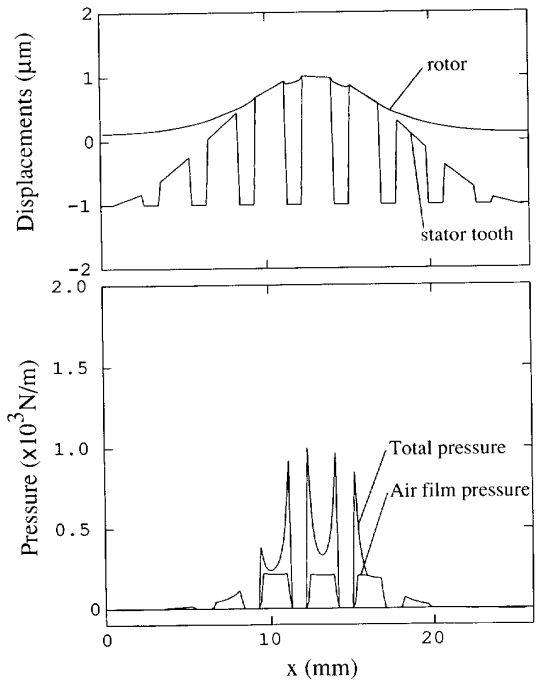

Fig. 6. Normal displacement and pressure distribution (minimum air bearing spacing = 100 nm).

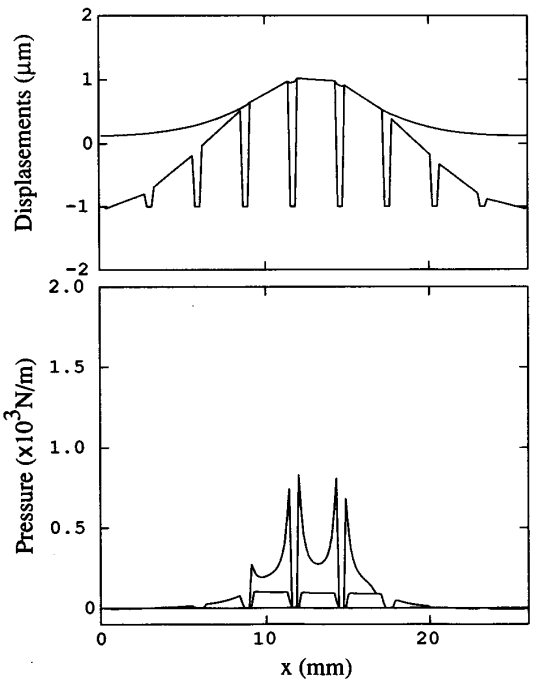

Fig. 7. Normal displacement and pressure distribution (tooth width = 2.31 mm).

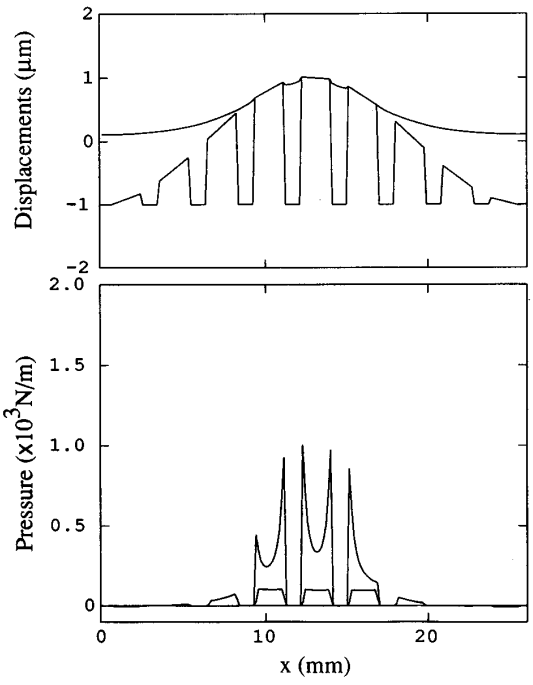

Fig. 9. Normal displacement and pressure distribution (Stator vibrating frequency = 100 kHz).

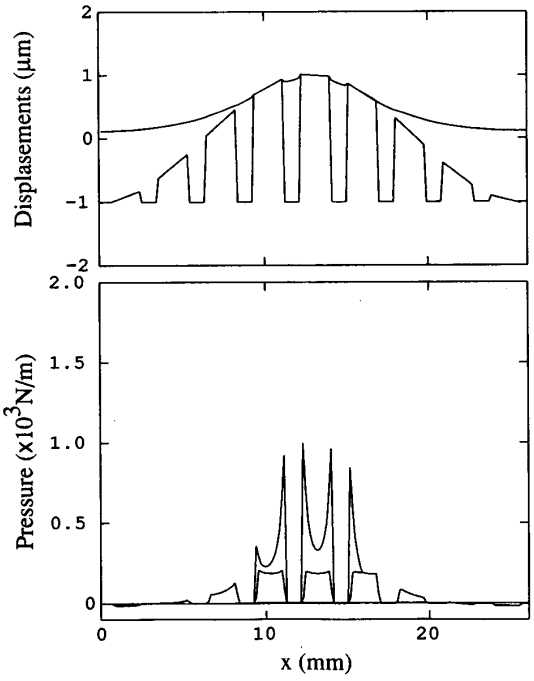

Fig. 8. Normal displacement and pressure distribution (rotor spring width = 0.6 mm).

C. Effect of Contact Area

Figs. 7 and 8 show the displacement of the rotor/stator and the pressure distribution when the teeth width is 2.31 mm and the rotor spring width is 0.6 mm, respectively. Results obtained for different teeth widths and the rotor spring widths show that the resultant hydrodynamic bearing pressure is proportional to the interface area of the rotor/stator under the ultrasonic frequency vibration. The smaller the interface area, the smaller the hydrodynamic bearing pressure ratio will be. On the other hand, a small contact area will cause a high contact pressure and large amount of wear per unit area. So an optimum interface area should be chosen by considering these two pressures. A motor whose stationary limiting torque is several times higher than the maximum operating torque could be designed by extending the interface area, because the hydrodynamic bearing appears only when the motor is driven. This prospect presents a new advantage of the ultrasonic motor when applied to high precision positioning mechanisms.

If the rotor stiffness is low, the contact area increases, and the hydrodynamic bearing pressure ratio α increases as well.

D. Effect of Vibrating Frequency

The effect of the stator vibrating frequency is studied by changing the stator frequency without changing the parameters, such as stator amplitude and rotor stiffness. Fig. 9 shows the normal displacement of the rotor/stator and the pressure distribution when the stator frequency is 100kHz. Fig. 10 shows the ratio α as a function of the vibrating frequency. When the frequency is higher, the normal velocity of the stator is higher and the squeeze effect is larger. If the frequency is changed without changing the rotational speed of the rotor, the change of normal velocity would be small, and

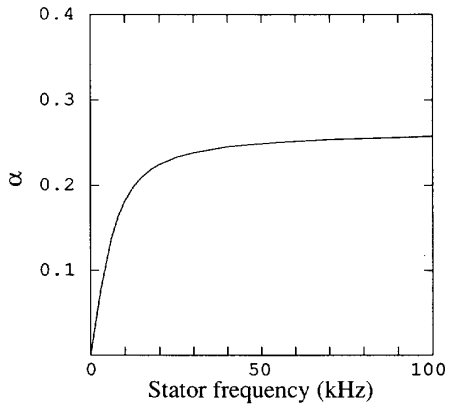

Fig. 10. Effect of stator vibrating frequency.

the hydrodynamic bearing effect might be almost the same as for the fundamental case.

E. Effect of Teeth Geometry

The previous calculation is performed by assuming that the rotor/stator surfaces are flat with sharp edges. But the actual macro geometry of a tooth surface is somewhat rounded at the edges and the pressure distributes more uniformly because of the wear, after it is driven for a few minutes. Therefore we made a calculation for curved teeth. When the arc radius is larger, the contact pressure distribution changes from the edge peaked shape to a half circle shape (See Fig. 12). When the radius of the teeth is 6.5 m, as shown in Fig. 11, the distribution of the contact pressure is almost uniform. This curve of the tooth surface corresponds quantitatively with the geometry of the actual tooth as shown in Fig. 5 (b). Looking at the hydrodynamic bearing, we found that the distribution of the pressure and the ratio α scarcely change.

IV. Conclusion

A hybrid numerical analysis including the hydrodynamic bearing effect and elastic contact in a ring-type ultrasonic motor is completed. The calculation is applied to various design parameters and the results can be summarized as follows:

1) Calculated results of the fundamental case show that the hydrodynamic bearing effect, especially the squeeze effect, on the rotor/stator contact is significant. A hydrodynamic bearing pressure ratio α was 0.24 in the fundamental calculation. It is somewhat small for explaining quantitatively the difference between the calculated and experimental values of μ in the previous study.
2) When the surface roughness of the rotor and stator are about 100 nm p-p each, α increases up to 0.48. In order to reduce the effect of the hydrodynamic bearing pressure, we must increase the interface surface roughness.
3) Results from changing the teeth width and the rotor spring width show that α is proportional to the interface area of the rotor/stator.

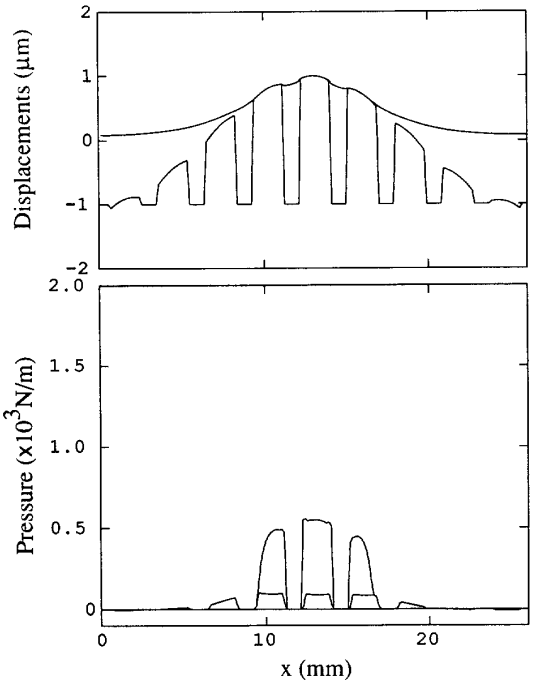

Fig. 11. Normal displacement and pressure distribution (teeth radius = 6.5 m).

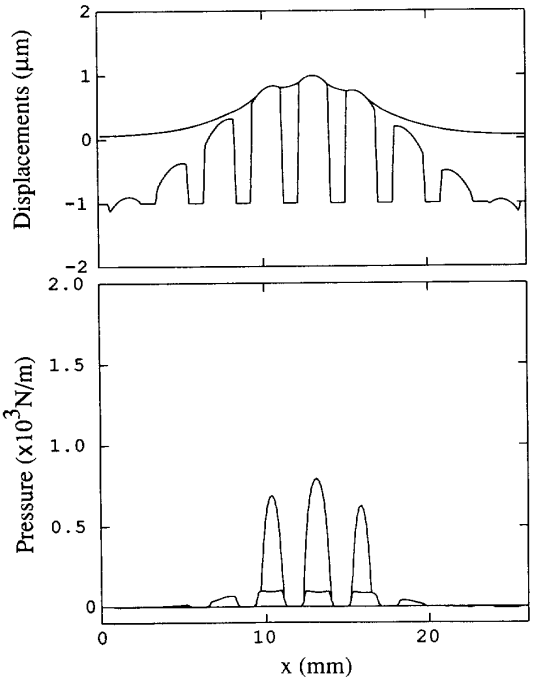

Fig. 12. Normal displacement and pressure distribution (teeth radius=3 m).

4) A low rotor stiffness leads to a large contact area and large α.
5) When the frequency is higher, the normal velocity of the stator is higher and the ratio α is larger.

6) When the arc radius of the teeth edges increases, the contact pressure distribution changes from the edge peaked shape to a half circle shape. On the other hand, the hydrodynamic bearing pressure distribution and the ratio α scarcely change.

ACKNOWLEDGEMENT

Takashi Maeno acknowledges Canon for supporting his sabbatical leave as a Visiting Industrial Fellow in CML.

REFERENCES

[1] T. Maeno, T. Tsukimoto, and A. Miyake, "Finite-element analysis of the rotor/stator contact in a ring-type ultrasonic motor," *IEEE Trans. Ultrason., Ferroelec., Freq. Contr.*, vol. 39, no. 6, pp. 668–674, 1992.
[2] T. Maeno, T. Tsukimoto, and A. Miyake, "Study on the contact mechanism of an ultrasonic motor," JSME Spring Annu. Meeting, 1990 (in Japanese).
[3] E. O. J. Salbu, *Trans. ASME* D, vol. 86, no. 2, pp. 335, 1966.
[4] K. Ono, "Analysis and its experimental verification of motion of mass supported on compressible squeeze film," *Trans. Japan Soc. Lubrication Eng.* vol. 21–9, p. 589, 1976 (in Japanese).
[5] J. W. White and A. Nigam, "A factored implicit scheme for the numerical solutions of the reynolds equation at very low spacing," *ASME J. Lubr. Tech.*, vol. 102, no. 1, pp. 80–85, Jan. 1980.
[6] D. Miu, "Dynamics of gas-lubricated slider bearings in magnetic recording disk files: Theory and experiment," Ph. D. dissertation, Univ. Calif., Berkeley, Dept. Mech. Eng., 1985.
[7] D. Miu and D. B. Bogy, "Dynamics of gas-lubricated slider bearings in magnetic recording disk files—Part II: Numerical simulation," *ASME J. Tribology*, vol. 108, p. 589, 1986.

Takashi Maeno, for a photograph and biography, please see page 674 of this TRANSACTIONS.

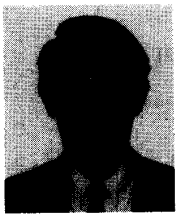

David B. Bogy (M'91) was born on June 4, 1936. He received the B.S. degrees in both mechanical engineering and geology in 1959, and the M.S. degree in 1961 from Rice University, Houston, TX, in 1959. After working for the Shell Development Company in Houston, TX, and serving in the Corps of Engineering of the U. S. Army he received the Ph.D. degree in applied mathematics in 1965 from Brown University, Providence, RI.

He was a postdoctoral fellow at the California Institute of Technology, Pasadena, during the 1965–1967 academic years, and joined the faculty in the Department of Mechanical Engineering at the University of California, Berkeley, in 1967. He founded the Computer Mechanics Laboratory at UCB in 1989. He became Chairman of the Department of Mechanical Engineering in 1991.

Dr. Bogy is a member of ASME.